cosmetics

MDPI

Article

Novel Crosslinked HA Hydrogel Films for the Immediate Release of Active Ingredients

Fatimah Rashid, Mustafa Albayati and Kalliopi Dodou *

Faculty of Health Sciences and Wellbeing, University of Sunderland, Sunderland SR13SD, UK
* Correspondence: kalliopi.dodou@sunderland.ac.uk

Abstract: Novel crosslinked hyaluronic acid (HA) hydrogel films were previously invented by reacting the HA polymer with the PT (Pentaerythritol Tetra-acrylate) crosslinker over basic pH conditions in the oven. HA is considered a natural polymer present in cosmetic as well as pharmaceutical formulations. This current study aimed to highlight the effect of loading method (post-loading and in situ) of selected actives (salicylic acid and niacinamide B_3) in the hydrogel films and then study their release kinetics. Differential scanning colometry (DSC) and Fourier transform infrared spectroscopy (FTIR) analysis evidenced the loading of the actives and full release from the HA hydrogel films, while the scanning electron microscopy (SEM) demonstrated the morphological changes to the films during the study by comparing the average molecular weight between crosslinks ($\overline{M}c$), gel fraction, crosslinking density (Ve) and mesh size (ξ) of the films. The loading percentage of the SA and B_3 showed high percentage loading of actives via both loading methods. In conclusion, the (95–100%) release of the actives achieved from the HA hydrogel films within 10 min revealed that the films are an efficient immediate release system of actives.

Keywords: hyaluronic acid; pentaerythritol tetra acrylate; hydrogels; cosmetics; niacinamide B_3; salicylic acid; DSC; FTIR; SEM

check for updates

Citation: Rashid, F.; Albayati, M.; Dodou, K. Novel Crosslinked HA Hydrogel Films for the Immediate Release of Active Ingredients. *Cosmetics* **2023**, *10*, 6. https://doi.org/10.3390/cosmetics10010006

Academic Editor: Enzo Berardesca

Received: 30 November 2022
Revised: 21 December 2022
Accepted: 22 December 2022
Published: 27 December 2022

Copyright: © 2022 by the authors. Licensee MDPI, Basel, Switzerland. This article is an open access article distributed under the terms and conditions of the Creative Commons Attribution (CC BY) license (https://creativecommons.org/licenses/by/4.0/).

1. Introduction

Hyaluronic acid (HA) has gained significant widespread usage by the cosmetic industry in limiting or reducing skin ageing [1]. Low molecular weight HA has dramatically shaped an important role in products that promote skin hydration. Whereas high molecular weight HA is widely used as filler to shape lips, contour cheeks and correct facial lines [2]. Thus, HA-based cosmetic formulations such as hydrogels, gels, dermal/intradermal filling injections, lotions, creams, and serums, have purported noticeable skin anti-wrinkle and anti-aging properties [3]. HA has favourable properties due to its biocompatibility, non-immunogenicity, and biodegradability [4]. It can also interact with receptors such as CD44, which is expressed in many types of tumour cells and accordingly, it is a candidate for delivery of imaging and anticancer agents [5]. HA can embed fibroblast growth factor and is used to make scaffolds, which can be used to fasten wound healing [6].

Hyaluronan is a non-sulphated glycosaminoglycan comprising repeating polymeric disaccharides of N-acetyl-D-glucosamine and D-glucuronic acid [7]. These are linked together by alternative beta-1, 3 and beta-1,4 glycosidic bonds [8]. It is a naturally occurring biodegradable polymer identical in molecular and chemical form in all tissues and has significant biological functions in all living cells [9].

HA is in powder form in its natural state, but due to its multitude hydroxyl and carboxyl groups, it is an effective gelling agent that can form a hydrogel when added to a liquid solvent under mild conditions [10]. The degree of crosslinking and modification determine its physical and chemical properties. Hydrogen atoms around the axis of the structure are non-polar and hydrophobic, while the side chains are more polar and hydrophilic [8]. The H-bonds stabilize the conformation of HA in solution. However, the

bonds are easily disrupted by temperature and pH. At intermediate pH levels, HA behaves like most other polymers with no strong intermolecular interactions, but as pH reduces towards 2.5, HA forms a gel due to decreasing carboxylate dissociation and increased intermolecular interaction [11]. HA must be chemically modified to form a less degradable gel that is used in many biomedical applications [11].

Type I hydrogels are crosslinked three-dimensional polymers holding hydrophilic groups in their structure able to retain water within their structure without dissolving [12]. Hydrogels may be made up of one or more polymers. The spaces between the macromolecules fill with water, swelling the compound to form a hydrogel. The polymers have hydrophilic functional groups which hydrate in aqueous media and are responsible for the hydrogels' ability to absorb water [13]. The crosslinks in the polymer network chains prevent dissolution of the hydrogel in water [14].

There are different types of hydrogels depending on their origin (natural versus synthetic hydrogels), polymer composition (copolymer, multipolymer and homopolymeric hydrogels), biodegradability (biodegradable hydrogels versus non-biodegradable hydrogels) and configuration (crystalline, non-crystalline, hydrocolloid aggregates, and semi-crystalline) [15,16]. Hydrogels can be categorized according to their type of crosslinking (chemical, biochemical and physically crosslinked hydrogels), physical appearance (matrix, microsphere, and matrix) as well as the network's electrical charge (neutral, anionic, cationic) [15,16]. Hydrogels can also be classified according to their method of preparation (homopolymer, copolymer, interpenetrating network, self-assembly, and semi-interpenetrating network) [15].

PT (Penta erythritol tetra acrylate) is a tetra-functional acrylate monomer widely used as crosslinker in polymerization. In previous studies, PT has been used as crosslinker for polyethylene oxide (PEO) via UV radiation [17] and for HA via exposure to high temperature (80 °C) in the oven [12]. Such crosslinked hydrogel films can be suitable for the delivery of drugs and cosmetic active ingredients by transdermal and topical (cosmetic) formulations, respectively, via application of the hydrogel film on the intact skin surface.

Vitamin B_3 is an important antioxidant in the body. It is vital in reducing the decline of NADH and NADPH, essential enzymes that play a significant function in the manufacture of cellular energy and lipids [18]. The anti-ageing role of Vitamin B_3 is attributed to the fact that these two enzymes often decline in number with age; when these enzymes are sufficiently present in the skin, they can create an effective defense mechanism against ageing-induced external factors. Vitamin B_3 also assists the skin in remaining hydrated as it encourages the production of natural emollients [19–21]. Niacinamide is an active amide form of vitamin B_3, and its chemical structure consists of 3-pyridine carboxamide. Due to vitamin B_3's excretion from the body without in vivo storage, it should be taken from various food sources and supplements [19]. Additionally, its small molecular size (122.1 Dalton) renders it a suitable active ingredient for transdermal delivery because it can diffuse systemically via the stratum corneum [22].

Salicylic acid is a nonsteroidal anti-inflammatory (mono-hydroxy benzoic acid) which is the active form of aspirin. It is widely used in the cosmetic sector to enhance skin beauty [23]. SA can exfoliate the dead skin cells (corneocytes) from the skin surface (stratum corneum) and it can also fade hyperpigmentations on the skin. Cosmetically, due to salicylic acid's UV radiation-induced conversion reactions, it has been used in sunscreen formulations where it can convert the harmful radiation waves into safer warmer long radiation waves [23]. Also, SA is keratolytic, which allows it to be utilized in wart healing [24] and as anti-comedogenic in acne. The carboxylic group in the SA structure allows H-bonding interactions with other ingredients and with structural polymers in pharmaceutical and cosmetic formulations, therefore enabling a high loading capacity in the vehicle [25]. The low molecular weight of SA (138 Dalton) enables its molecular diffusion via the stratum corneum for either a topical (cosmetic) or transdermal (pharmaceutical) effect.

The novelty of the HA hydrogel films was reported in our previous paper where we presented a new method of preparation of HA crosslinked hydrogel films, using PT

(pentaerythritol tetra acrylate) as the crosslinking agent under high temperature conditions (oven-assisted thermal crosslinking) in high pH [12]. The aim of this follow-up work was to investigate the efficiency of the crosslinked HA hydrogel film as a novel delivery system for pharmaceutical or cosmetic active ingredients; we achieved this aim via the following objectives: (i) feasibility of uploading basic and acidic active ingredients into the novel crosslinked HA hydrogel film via two different loading methods, (ii) characterisation of the properties of the loaded hydrogel films and, provided loading was successful, (iii) release behaviour of the active ingredient from the film.

2. Materials and Methods

2.1. Materials, Chemicals, and Reagents

Hyaluronic acid (HA) sodium salt with high molecular weight (1800–2200 KDa) was supplied by Infinity Ingredients (Binfield, UK), while PT (Pentaerythritol Tetracrylate) was purchased from Insight Biotechnology Limited (Middlesex, UK). Salicylic acid (SA) was purchased from BDH chemicals Ltd. Poole England and B_3 Niacinamide from Western Drugs Limited, Madri, Udaipur, India.

These materials were used as received unless otherwise described. Other chemicals and reagents included NaOH (1.0 M) and HCl (1.0 M), which were used for pH adjustment. Deionized distilled water was available in the laboratory and was used as solvent for the HA polymer gelling and as a polar swelling agent for the HA hydrogel films.

2.2. Preparation of Hyaluronic Acid Hydrogels

The preparation of hydrogel was carried out according to [12] with some changes to PT concentration. HA-based hydrogels were formulated with 5% *w*/*w* concentration of HA and 25% PT (to be noticed that the 25% PT was from the HA concentration. While in the whole film the PT concentration was 1.25% *w*/*w*). The hydrogels were prepared by dissolving HA in deionized distilled water; the mixtures were stirred with an IKA stirrer (IKA® Werke GmbH. & Co. KG, Staufen, Germany) for 24 h to obtain homogeneously mixed HA hydrogels. This was followed by adjusting the pH to alkaline (11–12) using a pH meter from Hanna instruments (a wireless pH tester for cosmetic creams). Then, PT was added, and the mixture was subsequently stirred slowly for 24 h to obtain completely homogenized HA-PT hydrogels. The hydrogel was left to stand for 48 h to release air bubbles before casting in Petri dishes. The cast hydrogel samples were air-dried at room temperature for four to five days. The obtained xerogel films were cut in small pieces ready for crosslinking.

2.3. Crosslinking Reaction

The oven-assisted thermal crosslinking of the HA-PT xerogel films was done using an 80 °C oven (Binder GmbH Bergster, 14 D-78532 Tuttlingen). The hydrogel film samples were placed in the oven for 24 h.

2.4. Hydrogel Swelling Studies

Three samples (n = 3) of the loaded xerogel films from each loading batch were accurately weighed (*Mo*) and then were swollen in distilled water for 24 h at room temperature. During swelling, the films were periodically removed from water; excess surface water was drip-dried, and the films were reweighed (*Ms*).

The percentage swelling (%) was calculated using Equation (1) [12]

$$\% \text{ swelling} = \frac{Ms - Mo}{Mo} \quad (1)$$

where *Mo* was the initial weight and *Ms* was the weight of the swollen hydrogel film at equilibrium.

The maximum swelling equilibrium (EWC) was calculated using Equation (2) [12].

After 1 h, they reached equilibrium.

$$\% \text{ EWC} = \frac{Ms - Mo}{Ms} \quad (2)$$

The gel fraction for each film was calculated using Equation (3)

$$\text{Gel Fraction } \% = \frac{Mr}{Mo} \quad (3)$$

where *M*r is the weight of film after drip-drying excess water.

2.5. Comparisons of Average MW between Crosslinks, Crosslinking Density, and Mesh Size

The average MW between crosslinks ($\overline{Mc}$), crosslinking density (*Ve*), and mesh size (ξ) of the medicated and unmedicated hydrogel formulations were calculated according to the equilibrium swelling theory, which assumes Gaussian distribution of crosslinked polymer chains. The Flory Rehner Equation (4) was used to calculate $\overline{Mc}$ [12].

$$Qv^{\frac{5}{3}} = \frac{\overline{v}}{v1}\overline{Mc}\left(\frac{1}{2} - x\right) \quad (4)$$

where $Qv^{\frac{5}{3}}$ is the volumetric swelling ratio, $\overline{v}$ is the specific volume of the dry polymer ($\overline{v}$ = 0.575 cm^3/g for HA), v 1 is the molar volume of the solvent (18 cm^3 /mol for water), and x is the Flory polymer solvent interaction parameter (for HA). The x value was estimated to be 0.473 based on several assumptions [13,25]. Qv was determined as Q_m, which is the degree of mass swelling, according to Equation (5).

$$Qv = 1 + Pp/Ps\ (Q_m - 1) \quad (5)$$

where, *Pp* is the dry polymer density (1.229 g/cm^3) and *Ps* is water density. Q_m is the swelling ratio using the weights of the films before (xerogel and loaded) and after swelling.

Q_m was used to calculate Qv. Equations (6) and (7) were used to calculate the effective crosslinking density (*Ve*) and swollen hydrogel mesh size (ξ), respectively.

$$Ve = Pp/\overline{Mc} \quad (6)$$

$$\xi = Qv\ \sqrt[1/3]{ro2} \quad (7)$$

where $\sqrt{ro2}$ is the root-mean square (RMS) distance between crosslinks, which is dependent on the MW between crosslinks. For HA, an RMS distance value was used as previously calculated (Equation (8)) [26].

$$(ro2/2\ n)\ ½ \cong 2.4 \text{ nm} \quad (8)$$

where n is the polymeric disaccharide units for HA with a given MW. For HA with an n of 5305 and MW of 2 × 106 g/mol, RMS was estimated as follows (Equation (9)).

$$\sqrt{ro2} = 0.1748\ \sqrt{\overline{Mc}}\ Qv\ 1/3(\text{nm}) \quad (9)$$

Then combining Equations (7) and (9) and substituting $\overline{Mc}$ for *Mn* gives Equation (10).

$$\xi = 0.1748\ \sqrt{\overline{Mc}}Qv\ 1/3\ (\text{nm}) \quad (10)$$

2.6. Active Loading Studies

B_3 and SA were loaded into the HA hydrogel films as model active cosmetic ingredients via two different methods shown in Table 1.

Table 1. Summary of the exact amount of model active added in the solution and active concentration inside the film in both methods of loading.

Loading Method	Amount of Active Added to Obtain Saturated Solution (gm/100 mL)	% Concentration of Active in the Film (% *w*/*w*)
B_3 post-loaded	37.5	45%
B_3 in situ	1	45%
SA post-loaded	0.19	-
SA in situ (i)	0.19	3.55%
SA in situ (ii)	1	45%

2.6.1. Post-Loading

Three replicates of unmedicated dry HA hydrogel films were immersed in saturated solutions at 32 °C for 24 h; solutions of B_3 and SA were prepared using distilled water as solvent. In order to obtain full saturated solutions, the amount of B_3 added was 37.5 gm and 0.19 gm for SA, respectively (Table 1). Preliminary studies showed that 32 °C and 24 h were the optimum conditions to ensure maximum active load [27].

After 24 h, the loaded hydrogel films were weighed and left for 24 h to dry. The dried loaded films were weighed, and the active load was determined by using Equation (1). This equation was adapted from Peppas et al., where the weight of active was considered [27].

$$\text{Active Loading (\%)} = (Md - Mo/Mo) \times 100\% \quad (11)$$

where *Mo* is the initial weight of xerogel while *Md* is the weight of active-loaded hydrogel films.

Regarding SA loading by osmosis method, preliminary studies showed the active did not load via this method. For this reason, the post-loading method for SA was not included in this paper.

2.6.2. In Situ Loading

HA/PT hydrogel films were loaded with either SA or vitamin B_3. The calculated amount of both actives (see Table 1) was weighed and dissolved in distilled water. HA was then added to the solution under intensive stirring, as previously described in the hydrogel preparation section. To compare both loading methods (in situ and osmosis method), the exact amount of both actives was included in the mixture formulations, based on the corresponding active's load obtained from immersions, as described in the post-loading method.

2.7. In Vitro Active Release Study

Active release studies were performed on selected active-containing hydrogel films from both loading methods in pH 7.4 PBS. The percentage of active release was evaluated by two methods at 32 °C [13].

Firstly, each film was placed in 100 mL phosphate buffer under gentle stirring using a magnetic stirrer. Five mL PBS samples were collected at different times, followed by topping up the volume with fresh PBS. The concentration of active released into the buffer was evaluated using a UV spectrometer via a beer-Lambert plot linear regression equation, and the percentage of cumulative release was plotted as a function of time. The wavelengths used for the detection of actives were 262 nm for B_3 and 296 nm for SA [28]. The measured absorbances were substituted in the calibration curve to obtain the amount of active released.

The percentage of cumulative active released was calculated using the Equation (12):

$$\text{CR\%} = \frac{Mr}{Md} \times 100 \quad (12)$$

where *Mr* is the amount of active released from the calibration curve and *Md* is the amount of active loaded in the film.

After completion of the study, the hydrogels were removed from PBS and left to dry. The dried xerogels were then accurately weighed, and the obtained weights were used to check the total percentage active release using Equation (13), which was adapted from Equation (1).

$$\text{Total percentage active release (\%)} = \text{MD} - \text{MR}/(\text{Weight of Loaded active}) \times 100\% \quad (13)$$

where MD is the weight of xerogel before the release study, MR is the weight of xerogel after the release study.

To calculate the percentage of ionization of the actives, films from all medicated and unmedicated formulations were chosen and swollen in distilled water. The pH values were measured with Janaway 3010 pH meter (Cole-Palmer Ltd., Staffordshire, UK). The percentage of ionization of the SA was calculated using Equation (14) [29].

$$\%\ \text{ionization (weak acid)} = \frac{10^{(pH-pka)}}{10^{(pH-pka)}+1} \times 100 \quad (14)$$

And the percentage of ionization of the B_3 was calculated using the Equation (15)

$$\%\ \text{of ionization (weak base)} = \frac{1}{1+10^{(pH-pka)}} \times 100 \quad (15)$$

Various release model kinetics equations were applied to all formulations:

Zero order Kinetics [30].

$$\frac{Mr}{Md} = \text{Ko}\ t \quad (16)$$

where $\frac{Mr}{Md}$ is the ratio of active release, t is the time and Ko is the zero-order release constant.

First order Kinetics [27].

$$\ln\ \frac{Mr}{Md} = \text{K1}\ t \quad (17)$$

where K1 is the first order release constant.

Higuchi model kinetics [31].

$$\frac{Mr}{Md} = \text{Kh}\sqrt{t} \quad (18)$$

where Kh is the Higuchi constant.

Korsmeyer-Peppas model [32].

$$\frac{Mr}{Md} = \text{Kp}\ t^n \quad (19)$$

where Kp is kinetic constant, n is the release exponent.

In Peppas model, the n value characterizes the release mechanism. Depending on (n) value, if (n) value = 0.5 is Fickian diffusion, $0.43 < n < 1$ indicates non-Fickian diffusion, while $n > 1$ refers to super case-II transport diffusion [30].

2.8. Fourier Transform Infrared Spectroscopy (FT-IR)

FT-IR was done at room temperature using the Shimadzu IR Affinity-1S Fourier Transform Infrared Spectrometer (Shimadzu UK Ltd., Milton Keynes, UK) for all hydrogel film batches to evaluate the active loading and release in the HA-PT xerogel films. FT-IR analysis was also carried for blank films and pure actives. The spectral range was 4000–550 cm^{-1} with the resolution set at 2 cm^{-1}.

2.9. Differential Scanning Calorimetry (DSC)

Differential scanning calorimetry experiments were performed using hermetic aluminium pans in DSC Q1000 thermal analyser (both TA Instruments, New Castle, DE, USA). The samples were analysed during three thermal cycles over 2.5 h. Pure actives and hydrogel film samples (xerogel and loaded) were weighed using a microbalance (Mettler-Toledo, Greifensee, Switzerland), placed in an aluminium hermetic sample pan, and closed with an aluminium lid: first cycle with a temperature range from 50 °C to 300 °C; second cycle with a temperature range from 300 °C to 50 °C; and third with a temperature range from 50 °C to 300 °C. All cycles were performed under liquid nitrogen (50 mL/min). Calibration was done using indium.

2.10. Scanning Electron Microscopy (SEM)

The morphology of hydrogel samples loaded with both loading methods, and films after the release study, were evaluated using a scanning electron microscope (Hitachi, Tokyo, Japan) operated in high-vacuum mode at an accelerating voltage of 5 kV. Prior to freeze drying, the swollen hydrogel samples were frozen in a −80 freezer and subsequently freeze-dried in an ALPHA 2-4/LSC device (Martin Christ Gefriertrocknungsanlagen GmbH, Osterode am Harz, Germany) under a vacuum of 0.1 Pa at −70 °C for 24 h to thoroughly remove the water. Due to HA's hygroscopicity, the vials were filled with nitrogen gas to keep the films away from moisture. The freeze-dried hydrogel samples were put into liquid nitrogen for few minutes, fractured with a razor blade to expose the internal structures, and stuck onto the sample holder. All samples were sputter-coated with gold and palladium using Agar sputter coater (AGAR-Scientific, Ltd., Stansted, UK) for 60 s before observation.

2.11. Statistical Analysis

All obtained data were expressed as mean ± standard deviation. Also, one-way analysis of variance (ANOVA) was used to compare the release percentage, swelling percentage, mesh size, and degree of ionization between the formulations. Differences within and between treatments were significant at an acceptable p value of < 0.05 ($p < 0.00001$).

3. Results and Discussion

3.1. Active Loading in the Hydrogel Films

SA and B_3 were chosen as cosmetic active ingredients to load in the HA hydrogel. The post-loading method of B_3 was successfully achieved with a high percentage of loading (>99%). The hydrophilic nature of B_3 is compatible with the HA polymer, while for SA there was no loading achieved by the osmosis method. Failure of loading was expected due to the negatively charged SA at high pH active repulsed by electrostatic interaction from the negatively charged HA [28,33].

The in situ loading method for B_3 in concentration (45%) w/w and SA in concentration (3.55%, 45%) w/w has been achieved. These active concentrations were chosen to be close to the concentrations of the osmosis method and thus easier to compare between them. However, SA was loaded in two different concentrations instead to evaluate the effect of active concentration in the films with the same loading method.

B_3 in higher concentration 37.5 gm was loaded in situ, but the film appeared low in mechanical strength. In contrast, the films which were loaded with 1 gm (45%) B_3 exhibited better appearance. Therefore, the former has been omitted from the study.

3.2. Swelling Behaviour of the Hydrogel Films

The swelling and crosslinking properties of the HA hydrogel films are summarized in Table 2. The blank unmedicated HA hydrogel films swelled rapidly and reached to equilibrium quickly. When the PT amount increased to 25% w/w (the ratio HA concentration), the swelling percentage was decreased. According to [12], there was a correlation between increasing the crosslinker and lowest percentage of swelling, Qv and ξ, mesh size [34].

Table 2. Summary of percent of loading, swelling, mesh size and cross-linking behaviour of all loaded hydrogel films.

Parameters	Unmedicated	Post-Loaded B_3	In Situ Loaded B_3	In Situ SA (i)	In Situ SA (ii)
% of Loading		96.10 (±0.04)	-	-	-
% of Gel fraction	88.88 (±1.55)	86.81 (±1.33)	63.48 (±2.36)	89.85 (±4.82)	54.08 (±0.96)
% Swelling	587.96 (±12.53)	405.22 (±51.66)	222.83 (±18.93)	529.09 (±24.31)	424.13 (±65.94)
%EWC	85.46 (±0.27)	80.10 (±1.69)	68.94 (±1.88)	84.08 (±0.61)	80.92 (±0.22)
Qv Volumetric swelling ratio	13.106 (±0.28)	9.03 (±1.00)	4.96 (±0.43)	11.79 (±0.54)	9.45 (±0.13)
$\overline{Mc}$ (g/mol/) Average molecular Weight between Cross-links	85,085.1 (±3018)	44,993 (±7025)	16,929 (±23,500)	71,408 (±5458)	49,363 (±1153)
Ve Crosslinking density Mol/cm^3	1.44×10^{-5}	2.77×10^{-5}	7.36×10^{-5}	1.73×10^{-5}	2.49×10^{-5}
ξ (nm) Mesh size	120 (±2.98)	78.83 (±8.31)	38.77 (±3.82)	106.2 (±5.69)	82.11 (±1.34)

From Table 2, the swelling behaviour, EWC, *Qv* of the loaded hydrogels showed differences in these parameters, especially the B_3 in situ loaded films showed significant difference from the unmedicated hydrogel films.

The lower percentage of swelling (405.55), ξ (38.77 nm), $\overline{Mc}$ (16929 gm/mol), *Qv* (9.03 ± 1.00) for the in situ B_3-loaded films could be due to the active being embedded inside the polymer matrices [17,27]. While Ve appeared higher (7.36×10^{-5}) for the in situ B_3-loaded films, the lower swollen mesh size ξ of hydrogel, the higher the crosslink density [12]. However, the percentage of swelling of both SA in situ loaded hydrogel films were close to the percentage of swelling of unmedicated hydrogel films. The percentage of gel fraction was decreased with increasing the actives' concentration.

3.3. Actives Release Study

To investigate the active's release from the HA films, quantitative drug detection was carried out via two methods: firstly, with UV absorbance measurements and secondly with hydrogel's weight difference before and after release.

Figure 1 shows the release of B_3 from films prepared using both loading methods. It was found that B_3 was released immediately from the HA hydrogel films, irrespectively to the loading method. Similarly, the release from the films for both SA (3.55%) and SA (45%) was rapid and completed in 10 min; our results were in agreement with results of [35].

The post-loading of B_3 showed over 99% release via both UV analysis and by weight difference. According to [33], the HA's high fluid uptake resulted in faster and complete release of the actives. This behaviour indicates that our crosslinked hydrogel is promising in the cosmetic sector and in wound dressing applications.

For the in situ loaded B_3 films (Table 3), the % release was 90.1% according to UV analysis measurements, while the weight difference showed higher release at 95.47%. This could be because of the positively charged B_3 (Table 4) retained in the negatively charged HA polymer, especially in the in situ loading method where the active was settled in the tortuous polymer structure, in contrast to the post-loaded B_3, where the morphologic study images with SEM revealed the active's presence in the microporous linear structure. See below SEM section.

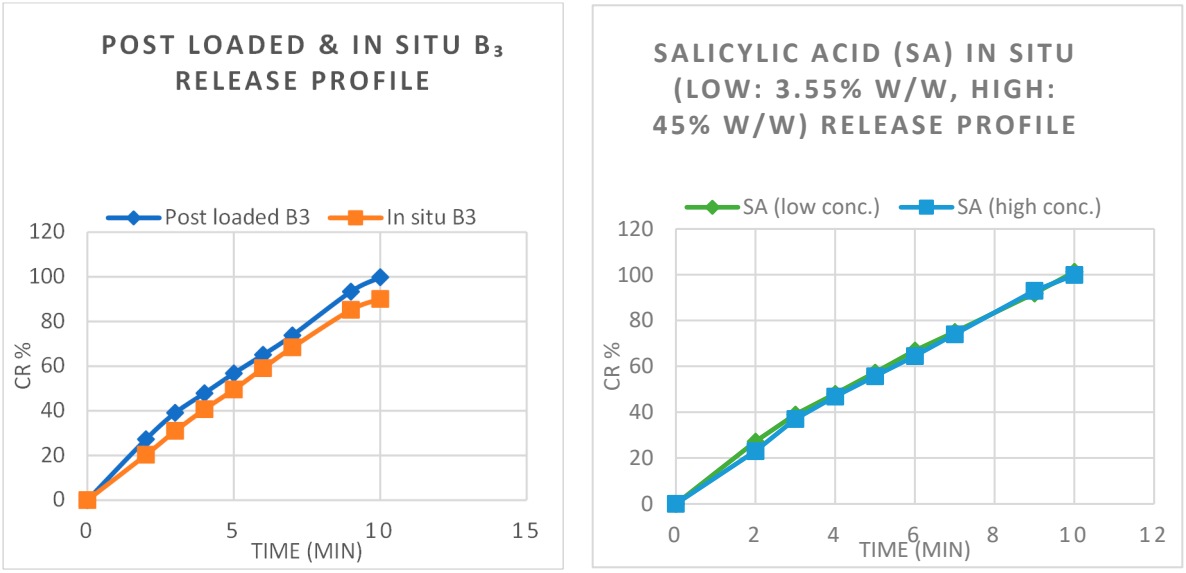

Figure 1. Actives B_3 and SA release profile (percentage release over time in minutes).

Table 3. Release data of all formulations.

Formulations	Active Concentration (% *w*/*w*)	Active Concentration (% *w*/*w*)	Mean Total Active % Release (Weight Difference)
Post-loaded B_3	45% (9 gm)	99.80 (±1.357)	100 (±0.00)
In situ loaded B_3	45% (1 gm)	90.1 (±2.54)	95.47 (±0.31)
In situ loaded SA (i)	3.55% (0.1907 gm)	101.3 (±2.32)	100.19 (±0.34)
In situ loaded SA (ii)	45% (1.025 gm)	99.86 (±2.16)	99.27 (±0.72)

Table 4. The percentage of ionization and pKa of the actives at the pH of the solution used for the loading method (deionized water).

Samples	pKa	PH of Solution	% of Ionization
Blank (unmedicated)	0	6.5	0
post B_3	3.35	7.11	0.017
insitu B_3	3.35	7	0.022
insitu SA (i)	2.97	6.5	99.97
insitu SA (ii)	2.97	8.1	99.999

When looking at the percentage of ionization of B_3 (Table 4), it is present in its non-ionized form, considering B_3 is a weak base, while SA being a weak acid had maximum ionization > 99% indicating that most of the active is solubilized in water.

Furthermore, the active release from the hydrogels could depend on different factors such as active's molecular size, charge, chemical structure, the polymer matrix morphology, and the polymer-active interactions [32]. This was indicated by the in situ loaded B_3 films' lower mesh size and higher Ve resulting in a lower percentage release than the other formulations. The explanation for this could be that B_3 could be bound with the HA polymer via stronger bonds. Therefore, its full release from the hydrogel would require the hydrogel's degradation [32].

Release kinetic models were applied to the release data to illustrate the actives' release kinetics from the hydrogel films (Figure 2a,b and Table 5). The R^2 values were employed for the determination of the best kinetic model for the release of each active from the films [36]. On Table 5, the highest R^2 is shown in bold for each film.

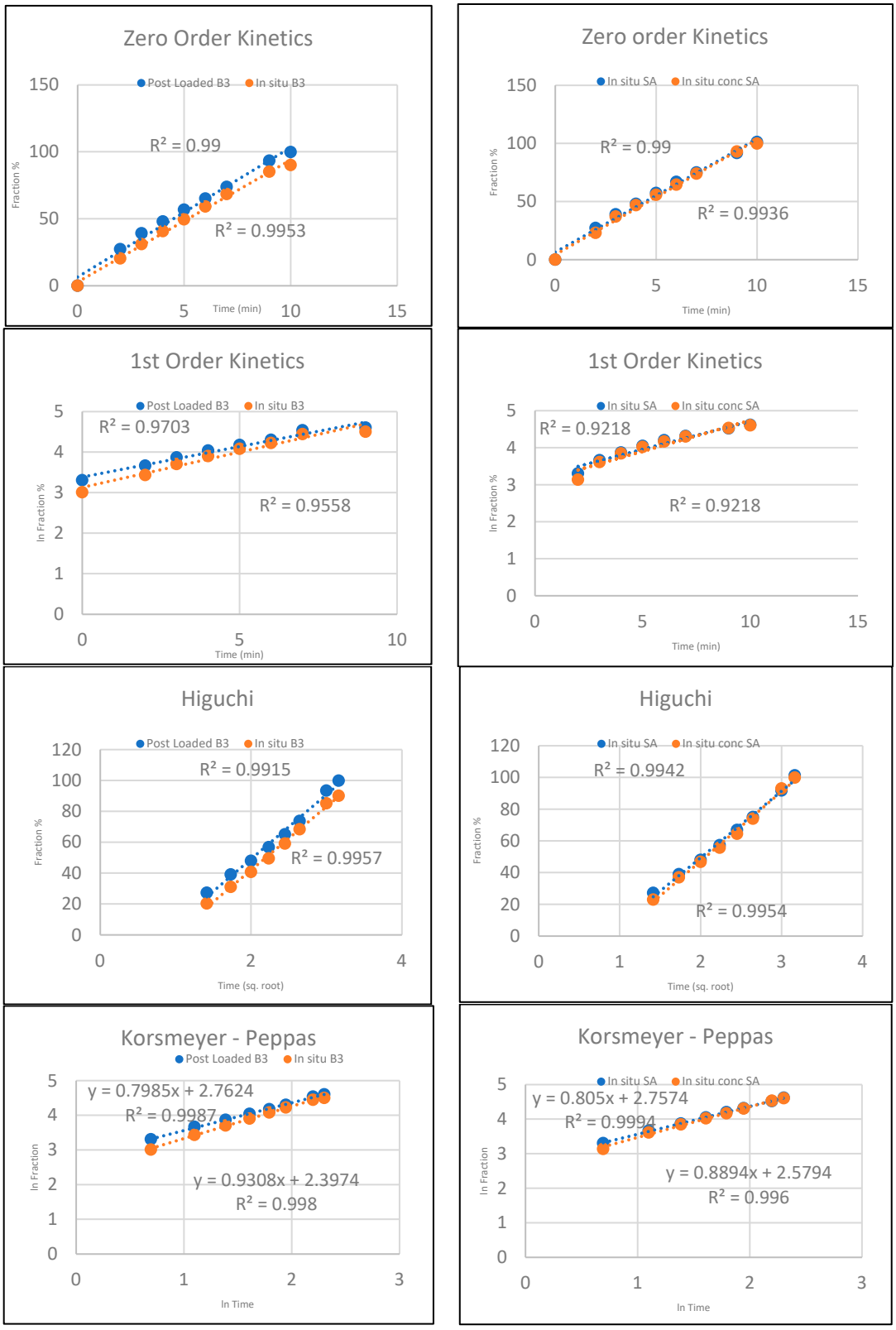

(**a**) (**b**)

Figure 2. (**a**) Drug release kinetics profile-B_3 (Post-loaded and in situ); (**b**) Drug release kinetics profile-SA (in situ and in situ conc.).

Table 5. Active release kinetics illustrate the (R^2), release rate constants (K) and release exponent (n) value for the formulations.

Kinetic Models	Zero-Order		First-Order		Higuchi		Korsmeyer–Peppas		
	K_0	R^2	K_1	R^2	KH	R^2	n	KKP	R^2
Post-loaded B_3	11.471	0.998	0.865	0.970	26.049	0.991	0.79	15.800	**0.998**
In situ loaded B_3	9.832	0.995	0.823	0.955	22.701	0.995	0.93	11.012	**0.998**
In situ loaded SA (i)	11.532	0.990	0.866	0.944	26.209	0.994	0.80	15.633	**0.999**
In situ loaded SA (ii)	11.039	0.990	0.851	0.921	25.352	0.995	0.88	13.183	**0.996**

It was found that the highest R^2 was with the Korsmeyer–Peppas model regardless of the loading method for B_3 and the concentration difference for the SA (Table 5). The n value for all the formulations was within the range of $0.5 < n < 1$, which indicated that the diffusion mechanism followed non-Fickian diffusion, where the active's release was via diffusion and hydrogel polymer chain relaxation [27,37,38]; the high swelling capacity of the crosslinked HA hydrogel films allowed the quick penetration of water into the polymeric network, the subsequent polymer expansion, followed by the active's quick dissolution, diffusion, and release from the hydrogel films. Our results agree with a recent study from Sang et.al [36] who reported that the immediate release of 5-Fluorouracil from crosslinked aerogels was also best described by the Korsmeyer–Peppas model.

3.4. FTIR Analysis

The FTIR analysis was carried out to all loaded and released hydrogel films, as well as the unmedicated hydrogel films with pure (HA and PT), to explore the molecular interactions inside the polymer films [39]. All FTIR spectra are presented in Figure 3. Hyaluronic acid polymer was successfully crosslinked with PT via an ester bond (C-O-C) between the hydroxyl group of the HA and the carbonyl carbon of the crosslinker PT. Initially the free radicals of PT are activated under alkaline conditions to generate nucleophiles which activate radical polymerization. The generated PT radicals abstract hydrogen atoms from HA to generate HA radicals which then bind with PT radicals to form crosslinks [12]. This reaction was illustrated in detail in our first paper [12]. Figure 3A shows that the stretching peak at around 1738 cm^{-1} in pure PT was reduced in intensity in the crosslinked blank hydrogel film, indicative of the reaction of the carbonyl group of PT with the hydroxyl group of HA, while the stretching peak around 1100–1300 cm^{-1} corresponding to (C-O-C) is the new bond (crosslink) between HA and PT.

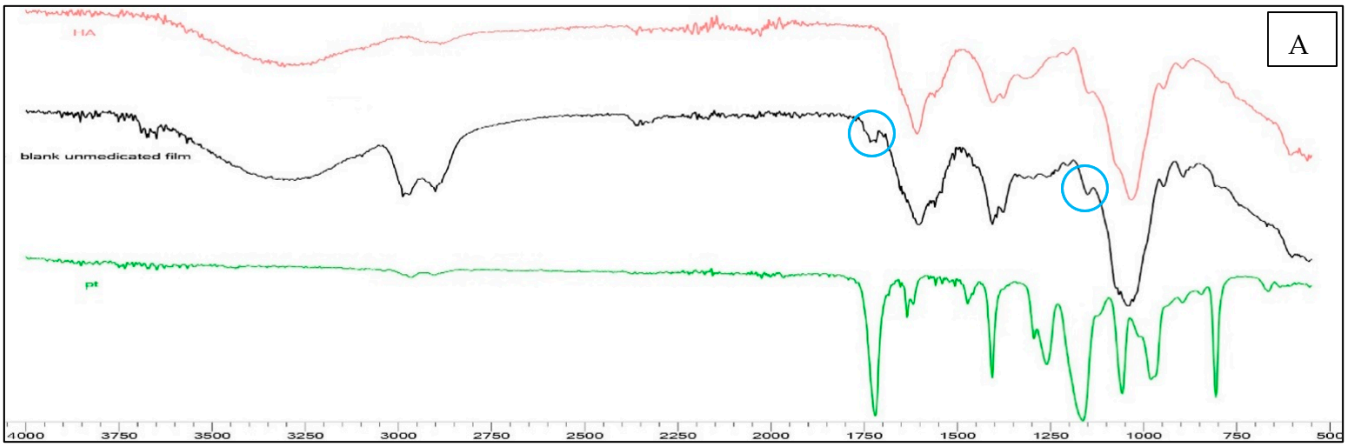

Figure 3. *Cont.*

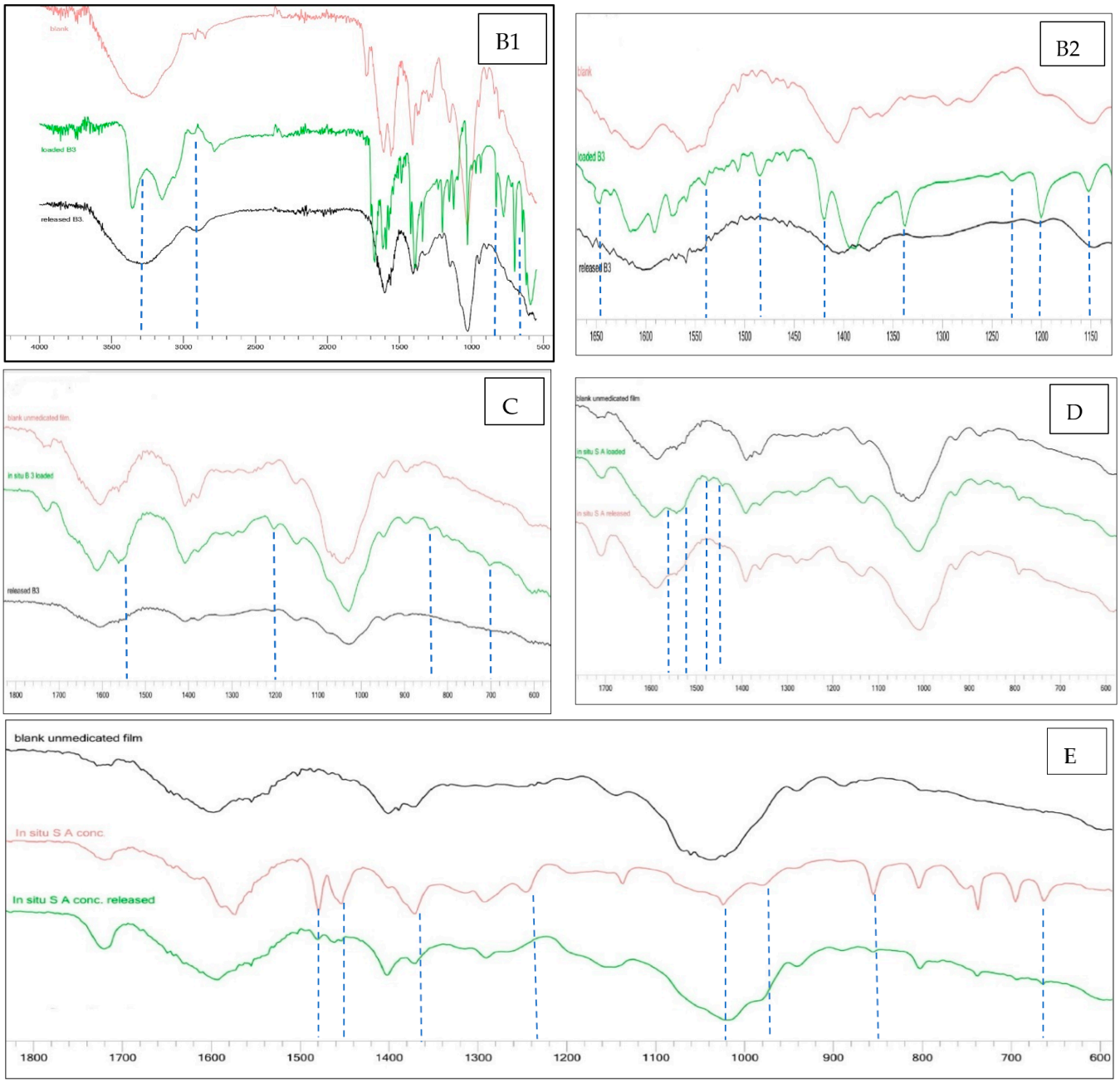

Figure 3. The FTIR spectra analysis for (**A**) compare blank unmedicated film with pure HA and pure PT, (**B1**,**B2**) post-loaded B_3 (to compare blank unmedicated film with loaded and released film from active). (**C**) In situ loaded B_3 profile (to compare the blank unmedicated film with active loaded and released film). (**D**) In situ 3.55% w/w SA (blank unmedicated film with active loaded and released film). (**E**) In situ 45% w/w SA (to compare blank unmedicated film with active loaded and released film).

The peaks around 2900–3300 cm^{-1} appearing in unmedicated film, stretched and disappeared in loaded B_3 films; this hydroxyl vibration region suggested the mixing of the active with the hydrogel polymer [33].

B_3-post-loaded spectra are shown in Figure 3A. The FTIR spectra of B_3-post-loaded hydrogel films exhibited new peaks at 1649, 1540, 1484, 1420, 1340, 1229, 1200 and 1150 cm^{-1} were (C=C, N-H, O-H, C-O) stretching, respectively [19,40]. These peaks indicated the presence of B_3 active in the hydrogel films, confirming the loading of the active, while the peaks ranged from (840–680) cm^{-1} were characteristic (C-H) totally related to B_3 peaks.

This also agreed with DSC and SEM, where the B_3 post-loading method showed less changes in the polymer structure.

Regarding the in situ loaded B_3 films (Figure 3B), the peak around 1540 cm^{-1} was C=C, while 1200 cm^{-1} belongs to C-O. Additionally, the 840, 700 cm^{-1} peaks from B_3 were detected as described in post-loaded B_3 bands. However, the post-loaded B_3 peaks were sharper than the in situ loaded B_3 peaks, which could be due to the stronger embedding of the drug in the polymer matrix using the in situ method [41].

SA 3.55% *w*/*w* in situ loaded hydrogel films exhibited strong N-O amide stretch in area 1520–1560 cm^{-1} [28]. Both (3.55%, 45%) *w*/*w* in situ loaded SA were recorded the C-H stretch in (1450–1480) cm^{-1} presented in Figure 3C,D. Notably, the peaks were sharper in 45% *w*/*w* SA in situ loaded films due to higher active concentration.

The FTIR spectra of 45% *w*/*w* in situ loaded SA evidenced bands at (96, 1018, 1240, 1460) cm^{-1} and symmetric C=C, strong C-O, C-N, C-H stretching. Obviously, the sharper peaks ranging from 660 cm^{-1} to 850 cm^{-1} in the 45% *w*/*w* in situ SA loaded film, were C-H band indicating the presence of SA in higher concentration.

Regarding the actives' release from all the loaded hydrogel films, the spectra showed complete absence of the actives' peaks after the release process, confirming that all active had been released.

3.5. DSC Analysis

DSC analysis was performed to investigate the thermal behaviour of the HA hydrogel films with and without actives. Firstly, the pure substances and the crosslinked xerogel films were analysed. Figure 4a shows the thermal curves of medicated films (loaded, released) and pure B_3 and the unmedicated crosslinked hydrogel film. The exothermic peak of blank (unmedicated) films was obvious around 240 °C which indicated polysaccharide degradation [33]. While the pure B_3 had an exothermic peak between 125–130 °C, this was suggested to Tm of the pure active in the first heating, which then disappeared on the second heating; presumably, it turned to an amorphous state [19].

However, the thermal DSC curve of the unmedicated crosslinked film has presented two different melting points, presuming impurities in the polymer. The broad endothermic peak at 80.75 °C was shifted toward the pure actives melting points after loading the films with actives, indicating the interaction with the polymer.

The sharp endothermic peak at (125.19–127.54 °C) was obtained in loaded B_3 via both loading methods, proving the presence of B_3 in the HA hydrogel films (Figure 4a,b). The main difference between in situ and osmosis loading was that the in situ B_3-loaded film kept the exothermic peak similarly to the unmedicated hydrogel; this could be attributed to the fact that the active was loaded inside the polymer matrices instead of settling in the porous structure; this was also confirmed by the SEM images, where the in situ B_3 loading caused marked changes in the HA hydrogel.

The analysis of DSC plots revealed that the thermal characteristics of the unmedicated film and the medicated film after B_3 release (Figure 1c) were relatively similar. The identical melting temperatures in cycle 1 and 3 and the crystallisation temperatures in cycle 2 suggested that the active was fully released from the films.

The pure SA showed (Figure 4c,e) a sharp melting endotherm peak in 158 °C, while in situ SA loaded (3.55%) presented Tm shifted to 161.61 °C and confirmed the SA presence altered the microstructure despite its low concentration. This was illustrated in the enlarged graph of loaded SA (Figure 4d).

Moreover, the in situ SA loaded in concentration (45% *w*/*w*) showed melting endotherm in 175.41 °C.

Concentrated SA in situ loaded 45% *w*/*w* exhibited another Tm in 238 °C. This referred to the presence of high crystalline active amount loaded in situ. Due to SA's lower solubility in water, the 45% *w*/*w* concentration was oversaturated in the solution used for producing the formulation. In addition, the presence of the various melting points can be explained by the presence of different polymorphic crystalline forms.

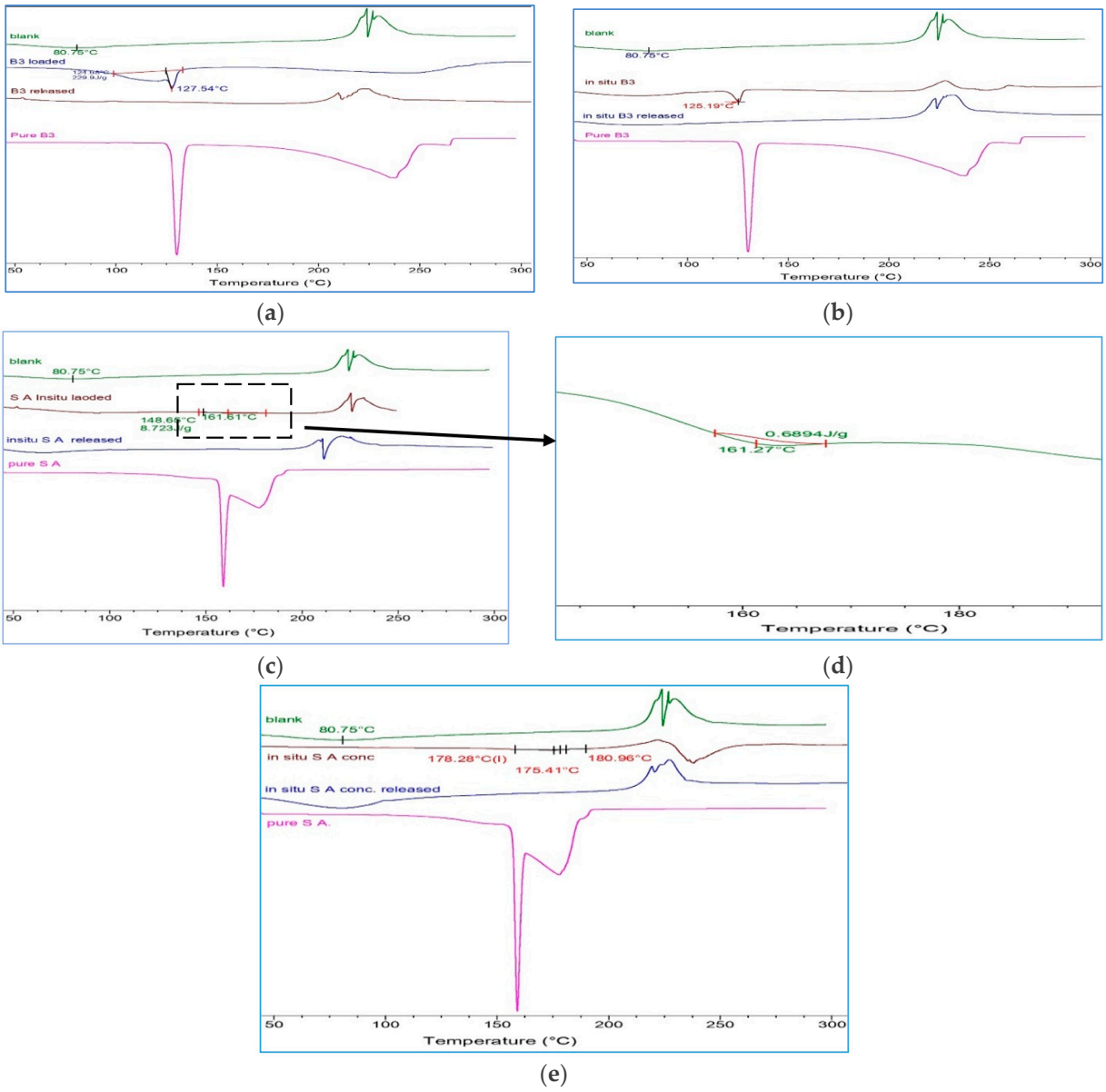

Figure 4. DSC thermograms (**a**) post-loaded B_3 (to compare the pure active, unmedicated film with loaded and released film from active). (**b**) In situ loaded B_3 (to compare the pure active, unmedicated film with active loaded and released film). (**c**) In situ 3.55% SA (to compare the pure SA, unmedicated film with active loaded and released film). (**d**) Enlarged in situ loaded 3.55% SA showing the thermogram peak of the SA. (**e**) In situ 45% *w*/*w* SA (to compare the pure active, unmedicated film with active loaded and released film).

However, the graphs for SA (3.55% *w*/*w*) and (45% *w*/*w*) films after release appeared similar to the unmedicated films, indicating that complete release has been achieved, in agreement with the release study results.

3.6. SEM

The morphological appearance of the unmedicated and medicated (loaded then released) hydrogel films has been studied with SEM. Figure 5(A1–A5) show the freeze-dried blank hydrogel films. It was obvious that the post-loaded B_3 films developed more micropores, and the mesh size was clearly larger in contrast to the in situ loaded B_3 where the active was immersed inside the polymer structure with lower mesh size (ξ). The mor-

phological appearance of the hydrogel films was particularly different when actives were loaded in situ [27].

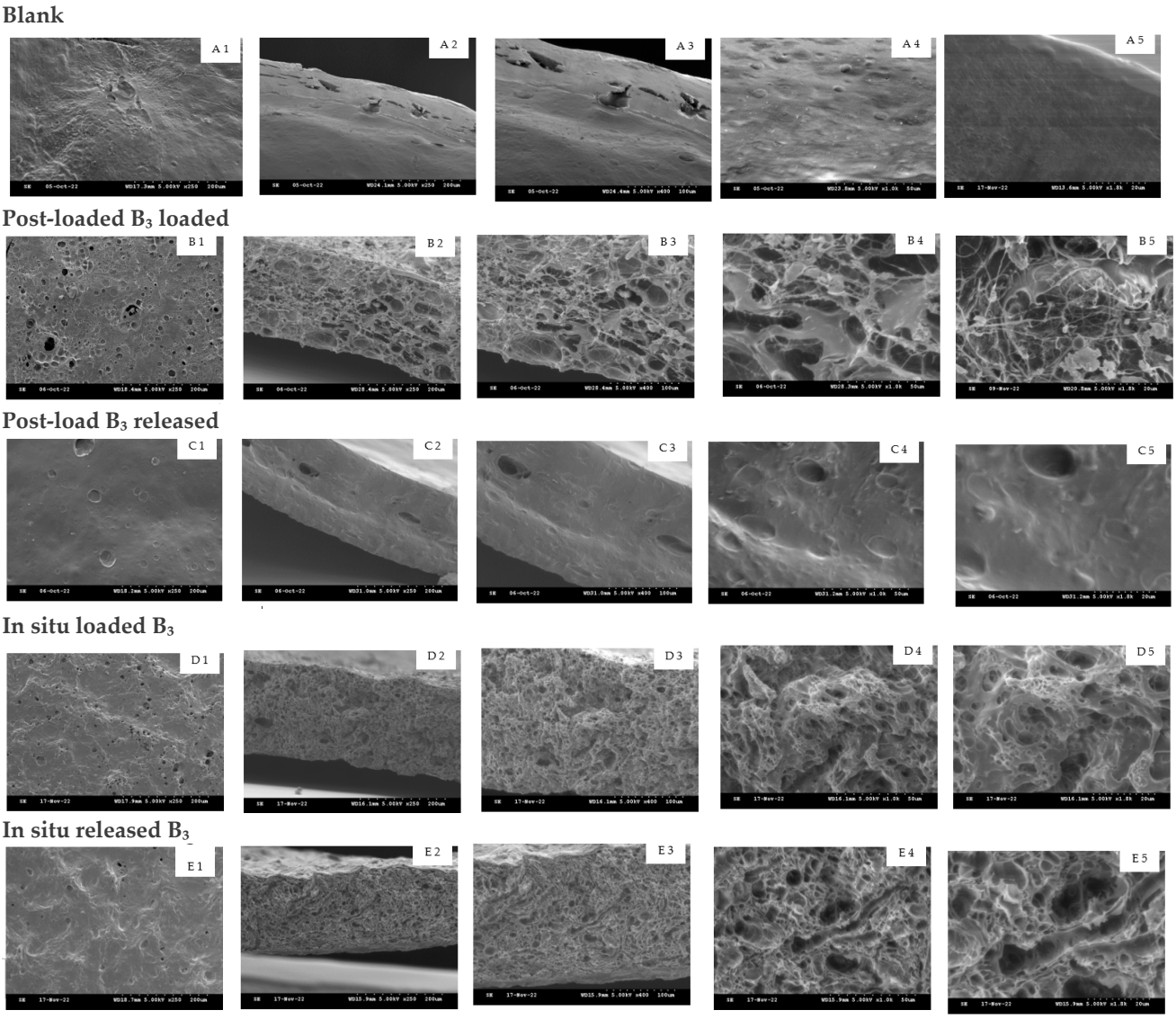

Figure 5. SEM images of the freeze-dried HA hydrogel films comparison. (**A1**–**A5**) blank (unmedicated) hydrogel film. (**B1**–**B5**) B_3 post-loaded hydrogel film. (**C1**–**C5**) B_3 post-loaded hydrogel film after release. (**D1**–**D5**) B_3 in situ loaded hydrogel film. (**E1**–**E5**) B_3 in situ loaded hydrogel film after release. The scale bars are 250 μm surface, 250 μm edge, 100 μm edge, 50 μm egde,10 μm edge.

Regarding SA, Figure 6(D1–D5) revealed the in situ loaded SA 45% *w*/*w* exhibited microporous structure with higher mesh size; moreover, these films were thinner. A possible explanation for this could be that more NaOH aqueous solution was added to the initial formulation to increase the pH to 11–12 for crosslinking; therefore, the polymer solution was diluted resulting in a thinner xerogel film upon drying [41].

However, after release, all hydrogel films with both actives demonstrated the spongy structure of the films except the post-loaded B_3, where the hydrogel films looked similar to the blank unmedicated films after B_3 release. This was explained by the active in post-loading not being embedded inside the polymer. In addition, B_3 could be interacting via ionic bonding with the polymer which allowed the active to release without significant change in polymer structure [27].

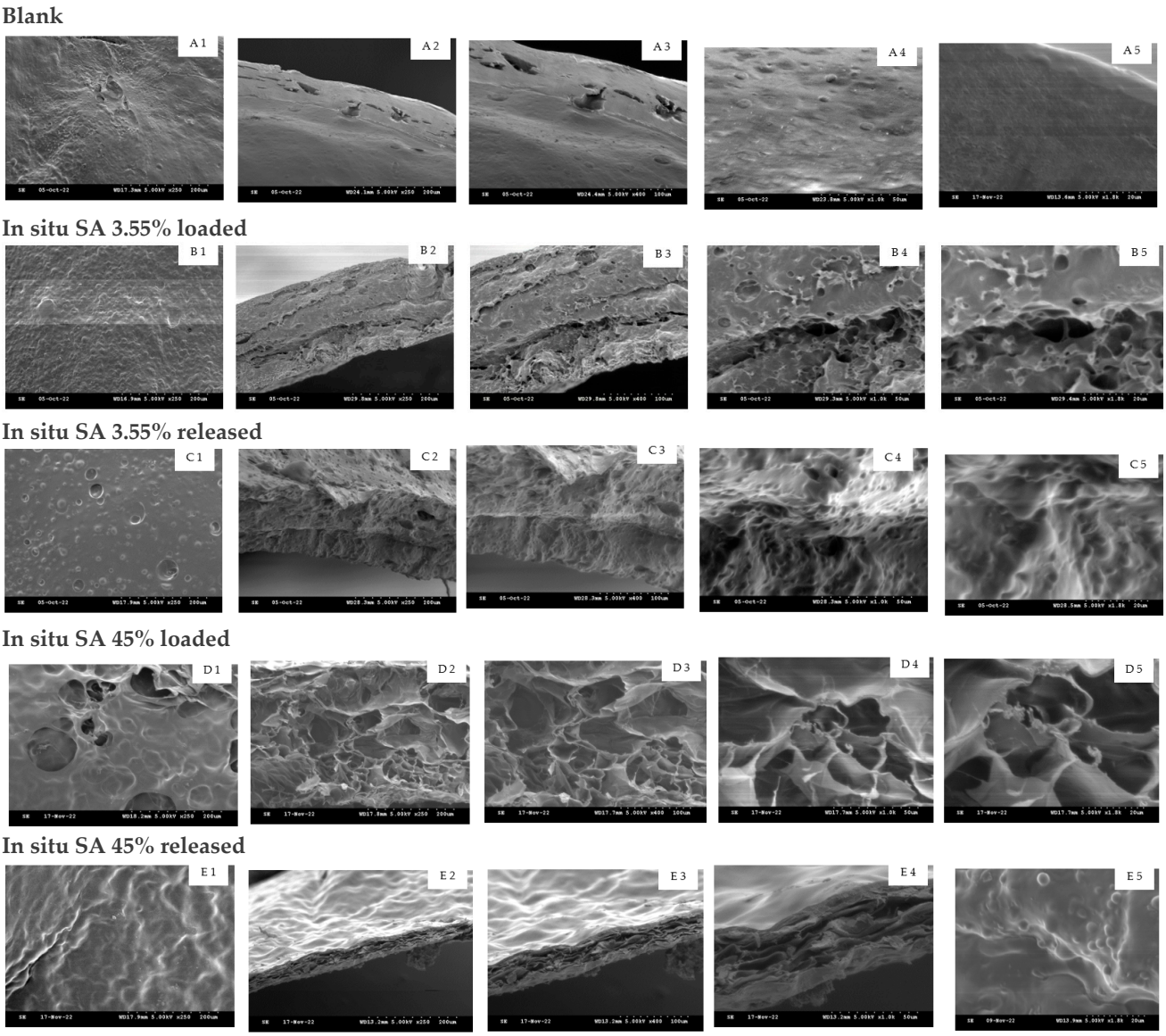

Figure 6. SEM images of the freeze-dried HA hydrogel films comparison. (**A1**–**A5**) blank (unmedicated) hydrogel film. (**B1**–**B5**) in situ SA 3.55% *w*/*w* loaded hydrogel film. (**C1**–**C5**) in situ SA 3.55% *w*/*w* loaded hydrogel film after release. (**D1**–**D5**) in situ SA 45% *w*/*w* loaded hydrogel film. (**E1**–**E5**) in situ SA 45% *w*/*w* loaded hydrogel film after release. The scale bars are 250 μm surface, 250 μm edge, 100 μm edge, 50 μm egde,10 μm edge.

The results of this study confirmed that the crosslinked HA hydrogel films can be suitable carriers for either acidic or basic low molecular weight ingredients. The complete in vitro release of the actives within 10 min indicates that these hydrogel films could potentially be useful for various cosmetic applications such as anti-ageing facemasks for the immediate release of active ingredients onto the skin, body patches for the local treatment of cellulite, etc., or pharmaceutical applications such as transdermal drug delivery and wound healing.

4. Conclusions

The drug-loading capacity of the novel crosslinked HA hydrogel films was examined using two different active ingredients (a weak base and a weak acid) via two different loading methods: in situ and post-loading via osmosis. The release kinetics of these actives from the films were also examined. It was found that loading and release from

the HA hydrogel films depend on the active's properties such as the solubility in water and ionisation status; the weak basic active could be loaded via either loading method, whereas the weak acidic active could be loaded only via the in situ method. The mechanical properties of the films (such as percentage of swelling, mesh size) were influenced from the loading method and drug-polymer interactions, as observed from the SEM, FTIR and DSC studies. The high percentage loading with both loading methods and the fast release of actives from the films, irrespectively of the loading method, revealed that these HA crosslinked hydrogel films are highly promising for cosmetic or pharmaceutical immediate release delivery systems.

Author Contributions: F.R. supervised by K.D.; K.D. conceptualized the work; experiments designed by K.D. and F.R.; F.R. performed the experiments; validation and evaluation by K.D. and F.R.; writing and drafting—F.R;. investigating and plotting, F.R. and M.A.; final reviewing, K.D. All authors have read and agreed to the published version of the manuscript.

Funding: This research received no external funding.

Institutional Review Board Statement: Not applicable.

Informed Consent Statement: Not applicable.

Data Availability Statement: Data is contained within the article.

Acknowledgments: We would like to thank Infinity Ingredients for their donation of the hyaluronic acid sodium salt.

Conflicts of Interest: The authors declare no conflict of interest.

References

1. Galus, R.; Antiszko, M.; Włodarski, P. Clinical applications of hyaluronic acid. *Pol. Merkur. Lek. Organ Pol. Tow. Lek.* **2006**, *20*, 606–608.
2. Olejnik, A.; Gościańska, J.; Nowak, I.; Faculty of Chemistry, Adam Mickiewicz. Significance of hyaluronic acid in cosmetic industry and aesthetic medicine. *CHEMIK* **2012**, *66*, 129–135.
3. Bukhari, S.N.A.; Roswandi, N.L.; Waqas, M.; Habib, H.; Hussain, F.; Khan, S.; Sohail, M.; Ramli, N.A.; Thu, H.E.; Hussain, Z. Hyaluronic acid, a promising skin rejuvenating biomedicine: A review of recent updates and pre-clinical and clinical investigations on cosmetic and nutricosmetic effects. *Int. J. Biol. Macromol.* **2018**, *120 Pt B*, 1682–1695. [CrossRef]
4. Huang, G.; Huang, H. Application of hyaluronic acid as carriers in drug delivery. *Drug Deliv.* **2018**, *25*, 766–772. [CrossRef] [PubMed]
5. Tripodo, G.; Trapani, A.; Torre, M.L.; Giammona, G.; Trapani, G.; Mandracchia, D. Hyaluronic acid and its derivatives in drug delivery and imaging: Recent advances and challenges. *Eur. J. Pharm. Biopharm.* **2015**, *97*, 400–416. [CrossRef]
6. Neuman, M.G.; Nanau, R.M.; Oruña-Sanchez, L.; Coto, G. Hyaluronic acid and wound healing. *J. Pharm. Pharm. Sci.* **2015**, *18*, 53–60. [CrossRef]
7. Papakonstantinou, E.; Roth, M.; Karakiulakis, G. Hyaluronic acid: A key molecule in skin aging. *Dermato-Endocrinol.* **2012**, *4*, 253–258. [CrossRef]
8. Necas, J.; Bartosikova, L.; Brauner, P.; Kolar, J. Hyaluronic acid (hyaluronan): A review. *Vet. Med.* **2008**, *53*, 397–411. [CrossRef]
9. Maneiro, E.; De Andres, M.C.; Fernández-Sueiro, J.L.; Galdo, F.; Blanco, F.J. The biological action of hyaluronan on human osteoartritic articular chondrocytes: The importance of molecular weight. *Clin. Exp. Rheumatol.* **2004**, *22*, 307–312.
10. Zhu, Z.; Wang, Y.-M.; Yang, J.; Luo, X.-S. Hyaluronic acid: A versatile biomaterial in tissue engineering. *Plast. Aesthetic Res.* **2017**, *4*, 219. [CrossRef]
11. Ström, A.; Larsson, A.; Okay, O. Preparation and physical properties of hyaluronic acid-based cryogels. *J. Appl. Polym. Sci.* **2015**, *132*, 42194. [CrossRef]
12. Rashid, F.; Albayati, M.; Dodou, K. Studies on Novel Methods for Formulating Novel Cross-Linked Hydrogel Films of Hyaluronic Acid. *Cosmetics* **2019**, *6*, 59. [CrossRef]
13. Akhtar, M.F.; Hanif, M.; Ranjha, N.M. Methods of synthesis of hydrogels. A review. *Saudi Pharm. J.* **2016**, *24*, 554–559. [CrossRef]
14. Ahmed, E. Hydrogel: Preparation, characterization, and applications: A review. *J. Adv. Res.* **2015**, *6*, 105–121. [CrossRef]
15. Bahram, M.; Mohseni, N.; Moghtader, M. *An Introduction to Hydrogels and Some Recent Applications*; IntechOpen: London, UK, 2016.
16. Singh, S.K.; Dhyani, A.; Juyal, D. Hydrogel: Preparation, Characterization and Applications. *Pharma Innov.* **2017**, *6*, 25–32.
17. Wong, R.S.H.; Ashton, M.; Dodou, K. Effect of Crosslinking Agent Concentration on the Properties of Unmedicated Hydrogels. *Pharmaceutics* **2015**, *7*, 305. [CrossRef]
18. Shimode, A.; Yagi, M.; Hagiwara, S.; Noguchi, T.; Inomata, M.; Kitano, S.; Yonei, Y. Anti-Glycation Activity of Alpha-Lipoic Acid Derivatives and Vitamin E Derivatives. *Anti-Aging Med.* **2013**, *10*, 42–54.

19. Basto, R.; Andrade, R.; Nunes, C.; Lima, S.A.C.; Reis, S. Topical Delivery of Niacinamide to Skin Using Hybrid Nanogels Enhances Photoprotection Effect. *Pharmaceutics* **2021**, *13*, 1968. [CrossRef]
20. Offerta, A.; Bonina, F.; Gasparri, F.; Zanardi, A.; Micicchè, L.; Puglia, C. In vitro Percutaneous Absorption of Niacinamide and Phytosterols and in vivo Evaluation of their Effect on Skin Barrier Recovery. *Curr. Drug Deliv.* **2016**, *13*, 111–120. [CrossRef]
21. Thomas, S.; Bharti, A.; Tharpa, K.; Agarwal, A. Quantification of potential impurities by a stability indicating UV-HPLC method in niacinamide active pharmaceutical ingredient. *J. Pharm. Biomed. Anal.* **2012**, *60*, 86–90. [CrossRef]
22. PubChem Compound Summery for CID 936, Nicotinamide. (n.d.). 3 1 2021. Available online: https://pubchem.ncbi.nlm.nih.gov/compound/Nicotinamide (accessed on 24 November 2022).
23. Arif, T. Salicylic acid as a peeling agent: A comprehensive review. *Clin. Cosmet. Investig. Dermatol.* **2015**, *8*, 455–461. [CrossRef] [PubMed]
24. Dainichi, T.; Ueda, S.; Imayama, S.; Furue, M. Excellent Clinical Results with a New Preparation for Chemical Peeling in Acne: 30 Salicylic Acid in Polyethylene Glycol Vehicle. *Dermatol. Surg.* **2008**, *34*, 891–899. [CrossRef] [PubMed]
25. Merinville, E.; Laloeuf, A.; Jalby, O.; Rawlings, A.V.; Morán, G. Exfoliation for sensitive skin with neutralized salicylic acid? *Int. J. Cosmet. Sci.* **2009**, *31*, 243–244. [CrossRef]
26. Baier Leach, J.; Bivens, K.A.; Patrick, C.W., Jr.; Schmidt, C.E. Photocrosslinked hyaluronic acid hydrogels: Natural, biodegradable tissue engineering scaffolds. *Biotechnol. Bioeng.* **2003**, *82*, 578–589. [CrossRef] [PubMed]
27. Wong, R.S.H.; Dodou, K. Effect of Drug Loading Method and Drug Physicochemical Properties on the Material and Drug Release Properties of Poly (Ethylene Oxide) Hydrogels for Transdermal Delivery. *Polymers* **2017**, *9*, 286. [CrossRef] [PubMed]
28. Niamlang, S.; Sirivat, A. Electrically controlled release of salicylic acid from poly(p-phenylene vinylene)/polyacrylamide hydrogels. *Int. J. Pharm.* **2009**, *371*, 126–133. [CrossRef]
29. Dodou, K.; Armstrong, A.; Kelly, I.; Wilkinson, S.; Carr, K.; Shattock, P.; Whiteley, P. Ex vivo studies for the passive transdermal delivery of low-dose naltrexone from a cream; detection of naltrexone and its active metabolite, 6β-naltrexol, using a novel LC Q-ToF MS assay. *Pharm. Dev. Technol.* **2015**, *20*, 694–701. [CrossRef]
30. Fallacara, A.; Marchetti, F.; Pozzoli, M.; Citernesi, U.R.; Manfredini, S.; Vertuani, A.S. Formulation and Characterization of Native and Crosslinked Hyaluronic Acid Microspheres for Dermal Delivery of Sodium Ascorbyl Phosphate: A Comparative Study. *Pharmaceutics* **2018**, *10*, 254. [CrossRef]
31. Marutpong, R.; Nophawan, P.; Anuvat, S.; Sumonman, N. Porcine and Fish Gelatin Hydrogels for Controlled Release of Salicylic Acid and 5-sulfosalicylic Acid. *Int. J. Drug Dev. Res.* **2015**, *7*, 107–117.
32. Ahsan, W.; Alam, S.; Javed, S.; Alhazmi, H.A.; Albratty, M.; Najmi, A.; Sultan, M.H. Study of Drug Release Kinetics of Rosuvastatin Calcium Immediate-Release Tablets Marketed in Saudi Arabia. *Dissolution Technol.* **2022**, *29*, GC1. [CrossRef]
33. Larrañeta, E.; Henry, M.; Irwin, N.J.; Trotter, J.; Perminova, A.A.; Donnelly, R.F. Synthesis and characterization of hyaluronic acid hydrogels crosslinked using a solvent-free process for potential biomedical applications. *Carbohydr. Polym.* **2018**, *181*, 1194–1205. [CrossRef]
34. Cui, N.; Qian, J.; Zhao, N.; Wang, H. Functional hyaluronic acid hydrogels prepared by a novel method. *Mater. Sci. Eng. C Mater. Biol. Appl.* **2014**, *45*, 573–577. [CrossRef]
35. Luo, Y.; Kirker, K.R.; Prestwich, G.D. Cross-linked hyaluronic acid hydrogel films: New biomaterials for drug delivery. *J. Control. Release Off. J. Control. Release Soc.* **2020**, *69*, 169–184. [CrossRef]
36. Sang, Y.; Pengpai, M.; Tao, C.; Yuan, Z.; Linfeng, C.; Yayang, T.; Xiaobing, H.; Jie, G. Fabrication and Evaluation of Graphene Oxide/hydroxypropyl Cellulose/chitosan Hybrid Aerogel for 5-fluorouracil Release. *Gels* **2022**, *8*, 649. [CrossRef]
37. Wojcik-Pastuszka, D.; Krzak, J.; Macikowski, B.; Berkowski, R.; Osiński, B.; Musiał, W. Evaluation of the Release Kinetics of a Pharmacologically Active Substance from Model Intra-Articular Implants Replacing the Cruciate Ligaments of the Knee. *Materials* **2019**, *12*, 1202. [CrossRef]
38. Jin, L.; Lu, P.; You, H.; Chen, Q.; Dong, J. Vitamin B12 diffusion and binding in crosslinked poly(acrylic acid)s and poly(acrylic acid-co-N-vinyl pyrrolidinone)s. *Int. J. Pharm.* **2009**, *371*, 82–88. [CrossRef]
39. Lewandowska, K.; Sionkowska, A.; Grabska, S.; Michalska, M. Characterisation of chitosan/hyaluronic acid blend films modified by collagen. *Prog. Chem. Appl. Chitin Its Deriv.* **2017**, *22*, 125–134. Available online: http://gateway.webofknowledge.com/gateway/Gateway.cgi?GWVersion=2&SrcAuth=ORCID&SrcApp=OrcidOrg&DestLinkType=FullRecord&DestApp=WOS_CPL&KeyUT=WOS:000424580500012&KeyUID=WOS:000424580500012 (accessed on 24 November 2022). [CrossRef]
40. Haxaire, K.; Maréchal, Y.; Milas, M.; Rinaudo, M. Hydration of polysaccharide hyaluronan observed by IR spectrometry. I. Preliminary experiments and band assignments. *Biopolymers* **2003**, *72*, 10–20. [CrossRef]
41. Kwon, S.S.; Kong, B.J.; Park, S.N. Physicochemical properties of pH-sensitive hydrogels based on hydroxyethyl cellulose-hyaluronic acid and for applications as transdermal delivery systems for skin lesions. *Eur. J. Pharm. Biopharm.* **2015**, *92*, 146–154. [CrossRef]

Disclaimer/Publisher's Note: The statements, opinions and data contained in all publications are solely those of the individual author(s) and contributor(s) and not of MDPI and/or the editor(s). MDPI and/or the editor(s) disclaim responsibility for any injury to people or property resulting from any ideas, methods, instructions or products referred to in the content.